Sensors and Materials, Vol. 33, No. 6 (2021) 2073–2082
MYU Tokyo

S & M 2594

Fabrication and Characterization of High-frequency Vibration Sensor over 6 kHz with Potential for Energy Harvesting

Lan Zhang,[1*] Ryohei Takei,[1] Jian Lu,[1] Daiji Noda,[2]
Ryo Ohta,[2] Takeshi Kobayashi,[3] and Toshihiro Itoh[1,4]

[1]Device Technology Research Institute, National Institute of Advanced Industrial Science and Technology (AIST), Tsukuba, Ibaraki 305-8564, Japan
[2]Micronano Open Innovation Center, Micromachine Center, Chiyoda, Tokyo 101-0026, Japan
[3]Sensing System Research Center, National Institute of Advanced Industrial Science and Technology (AIST), Tsukuba, Ibaraki 305-8564, Japan
[4]Department of Precision Engineering, University of Tokyo, 7-3-1 Hongo, Bunkyo, Tokyo 113-8656, Japan

(Received March 22, 2021; accepted May 11, 2021)

Keywords: vibration, MEMS, piezoelectric, high frequency, microsensors

We report on the fabrication and characterization of a high-frequency and high-voltage-output microelectromechanical systems (MEMS) vibration sensor with potential for energy harvesting. A novel structure was developed to ensure that the vibration sensor could output a high voltage in the high-frequency vibration domain. Specifically, the device was composed of eight aluminum nitride C-shaped spring flexures, which surrounded and supported a disk proof mass. The vibration sensor was fabricated, and its functional characteristics were comprehensively evaluated at a commercial foundry with an 8-inch MEMS process line. In experiments, the sensor exhibited an extremely high center resonance frequency of up to 6.7 kHz. Moreover, an output voltage of up to 167.8 mV was realized under an acceleration of 1 *g*.

1. Introduction

Vibrations are prevalent in modern social infrastructure systems. Although the effect of certain vibrations can be neglected, the effect of most vibrations must be taken into account because neglecting them may have critical consequences.[1,2] In this regard, vibration sensing approaches can be classified into low- and high-frequency domains. Many researchers have focused on the low-frequency vibrations of social infrastructure systems. Moreover, a vibration sensor for very low frequencies has been proposed.[3] Nevertheless, high-frequency vibrations can lead to failures owing to mechanical fatigue, and thus, such vibrations must be focused on. Under a high-frequency vibration environment, the target object load differs at various positions owing to specific structural characteristics. Therefore, numerous sensors must be applied on the target object to comprehensively monitor the vibration state. However, installing a large number of sensors may increase energy consumption. Thus, the development of techniques to simultaneously power multiple sensors and reduce power consumption is a key topic of interest.

[*]Corresponding author: e-mail: chou-ran@aist.go.jp
https://doi.org/10.18494/SAM.2021.3256

ISSN 0914-4935 © MYU K.K.
https://myukk.org/

In this context, renewable and inexpensive power sources can be exploited. In particular, solar and wind power have been efficiently and effectively used in several applications.[4,5] However, a solar cell cannot operate effectively in dark or indoor regions, and wind power generation requires a continuous stream of air. Notably, vibrations have correspond to a relatively high power density, especially in social infrastructure systems such as manufacturing compressors, elevator or escalator conveyors, and pump stations.[6,7] Thus, many techniques, such as those involving magnetic-energy harvesting,[8] electret-biased vibration-energy harvesting,[9] and piezoelectric harvesting,[10,11] have been developed and even commercially applied to harvest power from vibration sources. Among these techniques, the use of a MEMS-based piezoelectric gauge is a valuable powerless sensing approach. In particular, such devices can be seamlessly integrated in sensor systems or complementary metal oxide semiconductors because sensors are currently predominantly fabricated through MEMS processes. Moreover, the piezoelectric effect can not only serve as a direct and convenient energy source to realize the signal transmission of electromechanical information, but also help generate electric energy for the sensing system.[12,13] Previous relevant studies primarily focused on the vibration-energy-harvesting techniques for wireless, self-powered microsystems. Table 1 provides a comparison of various high-frequency MEMS vibration sensors with potential power-harvesting capabilities. The use of energy-harvesting MEMS sensors is an attractive research topic, especially with regard to their application in high-frequency sensing applications.

In this study, a high-frequency resonance sensor was developed to monitor the vibrations with potentially energy harvesting function from high-frequency vibration sources. The sensor developed in this study is based on a practical project need, that is, in a commercial central heat supply system; if the high-speed rotating machine in the system generates an abnormal working condition, it will produce particular high-frequency vibrations at several thousand hertz. Thus, we would like to discuss the viability of given high resonance frequency piezoelectric vibration sensors with narrow-band responses for predictive monitoring in this study. To satisfy the application requirements of high directivity and sensitivity, the vibration sensor was designed and fabricated with a novel structure involving a cylindrical proof mass attached and supported by eight AlN–silicon springs. Only the springs bent during the vibration, and owing to the symmetrical arrangement and mutual constraint of the springs, the proposed sensor was sensitive only to the external vibrations in the direction perpendicular to the structural plane.

Table 1
Comparison of high-frequency vibration sensors with potential energy-harvesting function.

	Resonance frequency (Hz)	Size (mm^2)	Output power / voltage	Features
Yu *et al.* [14]	234.5	3 × 2.4	66.8 W at 1 *g*	Multiple lead zirconate titanate (PZT) elements
Elfrink *et al.* [15]	200–1200 572 (typical)	5 × 5	60 μW at 2 *g*	AlN cantilever
Muralt *et al.* [16]	870	0.8 × 1.2	1.4 μW at 2 *g*	PZT cantilever
Kulkarni *et al.* [17]	8.08–9.83 k	5.7 × 6	23–296 nW at 1 *g*	Electromagnetic
Yaghootkar *et al.* [18]	>10 k	2 × 2	350 mV at 1 *g*	Diaphragm

Using optical techniques and an SEM, we investigated the microstructures of the fabricated sensors. Furthermore, we measured the deviation velocity amplitude of the forced vibration of the fabricated sensor to characterize the resonance frequency, which is a key mechanical property of sensors. Moreover, the sensor acceleration responsivity and the relationship between the sensor voltage output and the frequency in the sweeping domain were comprehensively evaluated. To verify the durability of the sensor, a temperature-cycling experiment was conducted. Finally, a preliminary application experiment was performed to verify the working capability of the proposed sensor.

2. Fabrication and Evaluation of Proposed Sensor

Silicon-on-insulator (SOI) wafers with 60-µm-thick active Si layers were used to fabricate the MEMS devices. The SOI wafers contained an oxide layer, through which 800 nm passivation was performed at the top, and a 1-µm-thick box layer between the active Si layer and substrate. Sandwiched layers of 250 nm/10 nm Pt/Ti, 1300 nm AlN, and 500 nm/10 nm Pt/Ti as the bottom electrode, piezoelectric layer, and top electrode, respectively, were deposited on the top surface of the SOI wafer by sputtering. Photolithography and metal etching were used to pattern and dry etch the sandwiched layers with high precision. Inductively coupled plasma–reactive ion etching (ICP-RIE) was performed to prepare the spring-beam flexures and release the proof mass from the backside of the wafer.

Figure 1 shows an image of the developed sensor, with a one-cent Euro coin shown for comparison to illustrate the die size of the developed sensor. The vibration sensor contained micromachined sandwiched AlN C-shaped gauge springs, which surrounded a flat cylindrical

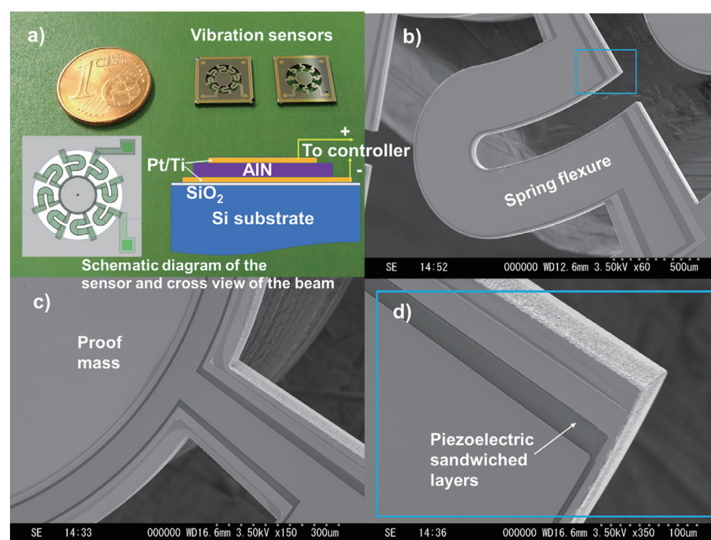

Fig. 1. (Color online) (a) Fabricated piezoelectric high-frequency resonance vibration sensors, insets are schematic illustrations of the vibration device design, and sandwich structure electrical interconnections. (b)–(d) Magnified SEM images of the fabricated sensor MEMS structures.

proof mass. The principle of this particular design was as follows: A large cylindrical proof mass was attached to eight AlN–silicon C-shaped beam flexures. The proof mass was considerably thicker than the C-shaped beams; consequently, during vibration, only the beams were expected to bend, and a symmetrical placement was implemented to ensure that the proof mass was sensitive only to the external vibrations in the direction perpendicular to the structural plane. The proof mass was designed and fabricated with six different diameters: 2.5, 3, 3.5, 4, 4.5, and 5 mm. As shown in Fig. 1(a), the typical vibration sensor included a proof mass with a diameter of 3 mm and eight C-shaped beam flexures with a length of approximately 940 or 2000 μm. The flexure lengths could be changed to adjust the center resonance of the target sensor to impart certain desirable characteristics. Figures 1(b)–1(d) show SEM images of the fabricated sensor microstructures. The piezoelectric transducers were deposited onto the individual springs, which were connected to one another through a circular circuit at the edge of the proof mass [Fig. 1(c)]. Precise microstructures of the piezoelectric sandwiched layer were realized through MEMS fabrication processes [Fig. 1(d)].

In the fabrication, sputtering equipment (SME-200E, Ulvac Co., Ltd.) was used to deposit the piezoelectric and metal layers. A metal etcher (E-658, Panasonic Co., Ltd.) was used to generate the sandwiched layers by etching the piezoelectric and metal layers. Dry etching equipment (E-628, Panasonic Co., Ltd.) was used to pattern the passivation layers of SiO_2. An ICP-RIE etching system (MUC-21, SPP Technologies Co., Ltd.) was used to dry etch the wafer to release the sensor structure.

An integrated test system composed of a controller (CS-18 compact, Spektra Inc.), a vibration exciter (SE-10, Spektra Inc.), and an amplifier (PA14-180, Spektra Inc.) was used to evaluate the performance of the fabricated vibration sensors. A laser Doppler velocimeter (LDV) (MLD-221D, Neoark Co.) was used to characterize the deviation amplitude of the fabricated sensors at the resonance frequency. An SEM (S-3000H, Hitachi Co., Ltd.) was used to observe the microstructure of the fabricated sensors.

3. Measurement Results

3.1 Mechanical measurement

The details of a similar MEMS device measurement system and the sensor settings have been provided in our previous work.[3] In this study, the response of the deviation velocity amplitude in the sweeping frequency domain was determined for the fabricated sensors. Figure 2 shows the resonant peaks of the fabricated short-beam sensor with proof-mass diameters ranging from 2.5 to 5 mm in intervals of 0.5 mm. By decreasing the proof-mass diameter from 5 to 2.5 mm, the resonance frequency increased from 3995 to 6768 Hz.

The sensor included multiple flexures to support the proof mass. Consequently, the first-mode resonance of the sensor was in the out-of-plane perpendicular direction with a large amplitude. Moreover, the second resonance mode corresponded to an in-plane vibration with a limited amplitude. After the first-mode resonance occurred, forced oscillation spectral lines dominantly appeared in the output signals (Fig. 2). The in-plane flattening or rotation

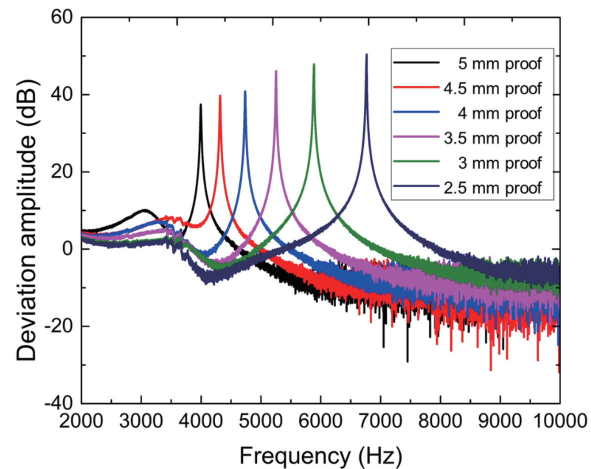

Fig. 2. (Color online) Measured responses of the short-beam device for different frequencies and proof-mass diameters.

deformation was restricted to have a limited amplitude; consequently, at a certain frequency, the proposed sensor could effectively harvest the energy of the ambient vibrations.

In addition, we evaluated the resonant peaks of the long-beam sensors with different proof-mass diameters. The resonance frequencies ranged from 2578 to 5504 Hz. The variation trend was similar to that of the short-beam sensors; specifically, the resonance frequency increased as the proof-mass diameter decreased. Moreover, when the sensor flexure beam was extended, the resonance frequency of the device sharply decreased. Nevertheless, as the long-beam sensor underwent a larger flexure deformation under the same acceleration, a marginally larger output was obtained.

The mechanical properties (Q-value and weight) of typical devices with different proof-mass diameters were examined. In general, the Q-value is the ratio of the device resonance frequency to the bandwidth of the resonant peak at a power of −3 dB. The Q-values of the vibration sensors with a short-beam flexure were measured in a linear range from 363.2 to 752.0. The long-beam-flexure sensors exhibited Q-values of 368.3, 490.3, 282.5, and 393.0 for the proof-mass diameters of 5, 4.5, 4, and 3.5 mm, respectively. In the case of the long-beam-flexure sensors, the nonlinear effects were considerable owing to the complex vibration modes in such sensors. In general, the power density of a vibration-derived energy-harvesting device is proportional to the Q-value. Moreover, a higher Q-value indicates a lower rate of energy loss relative to the stored energy of the oscillator. Thus, it is considered that the fabricated vibration sensors were sufficiently sensitive to monitor specific high-frequency vibrations with a high output power.

3.2 Electrical measurement

The electrical properties of the fabricated vibration sensors were examined. The characteristics of two typical 2.5-mm-diameter proof-mass sensors with short and long beams

were compared. The testing system involved an analog-to-digital converter (ADC) with high precision, which could convert the analog voltage data of the sine wave into an effective root mean square (RMS) value. Figure 3 shows the tested output voltage of the short-beam sensor responses under different acceleration values. The RMS voltage ranged from 4.3 to 36.6 mV under a load acceleration ranging from 0.1 to 1 g. As the peak-to-peak (p-p) analog sensor voltage is $2\sqrt{2}$ times the RMS value, the sensor device had p-p voltages of 12.2 and 103.5 mV under accelerations of 0.1 and 1.0 gravitational force equivalent, respectively. The gravitational force (*g*) was set with a value of 9.8 m/s^2. Moreover, the developed sensor exhibited a constant center resonance frequency as the acceleration increased, although the output response domain increased accordingly.

Figure 4 presents the measured acceleration responsivity and output voltage under different acceleration values. The output voltage increased as the acceleration increased but the measured acceleration responsivity decreased. This phenomenon occurs because as the vibration amplitude increases, the piezoelectric gauge deformation increases; however, when nonlinear deformation occurs in the case of a short-beam flexure, the piezoelectric gauge cannot necessarily maintain a consistent change rate for different acceleration values.

Figure 5 shows the measured output voltage of the long-beam sensor under different acceleration values. After the RMS–ADC conversion, the output voltage of the long-beam sensor ranged from 9.06 to 74.8 mV, corresponding to load accelerations from 0.1 to 1 *g*, respectively. Figure 6 shows the measured acceleration responsivity and output voltage under different acceleration values. The variation trends were similar to those shown in Fig. 4. As the vibration acceleration increased, the output voltage increased and the acceleration responsivity decreased. However, because the developed sensor with a long-beam flexure exhibited a larger linear deformation than the short beam, a consistent responsivity could be maintained at lower acceleration values (up to 0.3 *g*) as shown in Fig. 6.

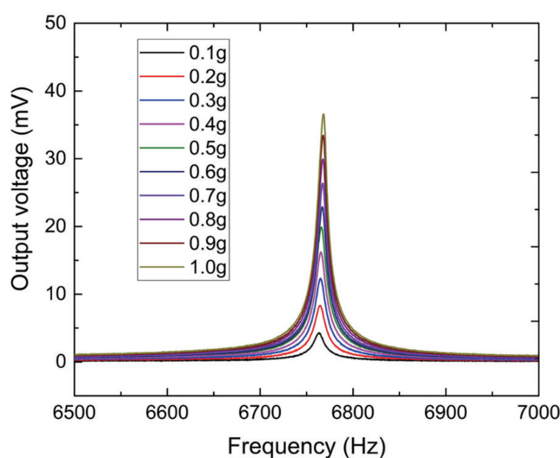

Fig. 3. (Color online) Measured output voltage of the device (2.5 mm proof mass with a short beam) under different acceleration values.

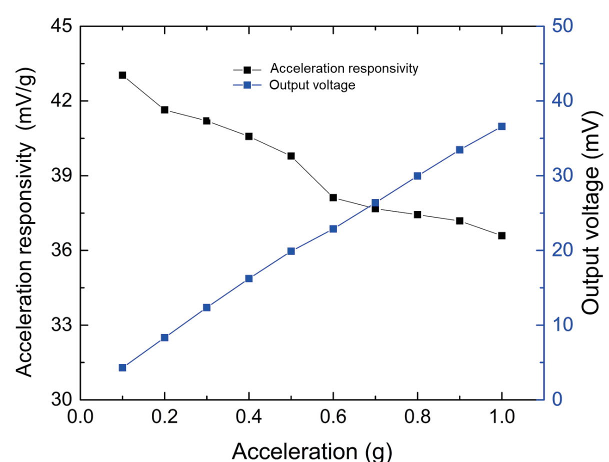

Fig. 4. (Color online) Measured acceleration responsivity and output voltage under different acceleration values (short-beam sensor).

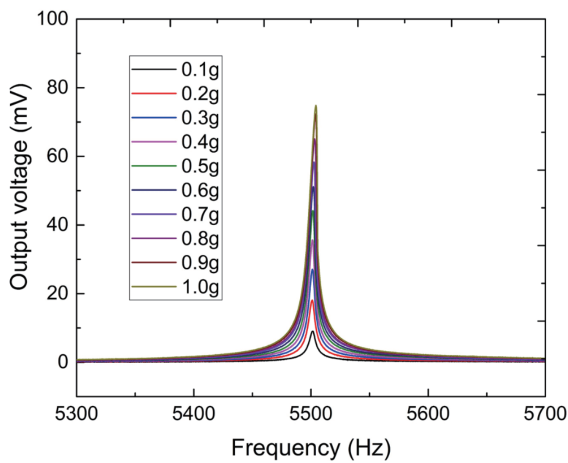

Fig. 5. (Color online) Measured output voltage of the device (2.5 mm proof mass with a long beam) under different acceleration values.

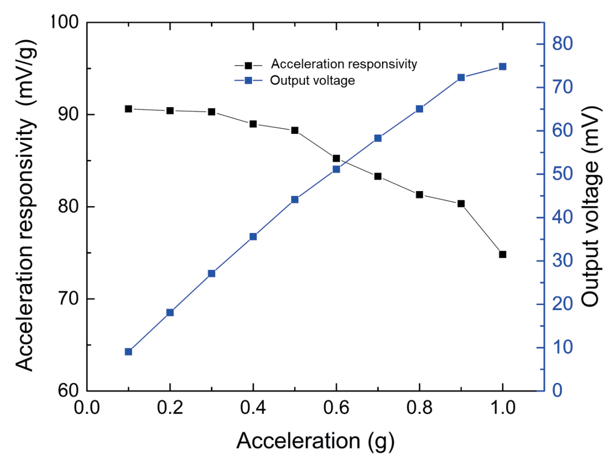

Fig. 6. (Color online) Measured acceleration responsivity and output voltage under different acceleration values (long-beam sensor).

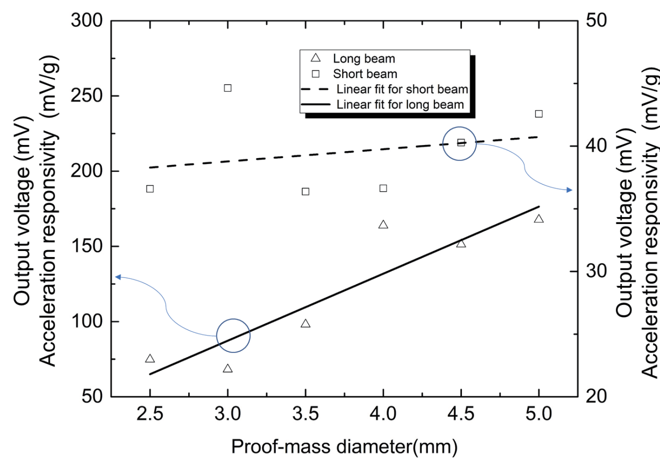

Fig. 7. (Color online) Output voltage of the short- and long-beam sensors with different proof-mass diameters under an acceleration of 1 *g*.

Figure 7 shows a comparison of the relationship between the measured values of the generated output voltage and the proof-mass diameter for the two different device geometries (short- and long-beam flexures). Because the acceleration was set as 1 *g*, the longitudinal coordinates could represent the output voltage and the acceleration responsivity. The results showed that the short-beam flexure sensors with the proof masses with diameters ranging from 2.5 to 5 mm could generate a maximum DC voltage output ranging from 36.6 to 42.6 mV, respectively. The corresponding maximum DC voltage output for the long-beam flexure sensors ranged from 74.8 to 167.8 mV. Notably, under the same acceleration, the longer beam underwent greater deformation (having a greater effect on the piezoelectric gauge) than the short-beam sensor, resulting in the generation of a higher voltage. Another reason for this finding is the

coating of the AlN film on the spring flexure, owing to which compressive strain and tensile strain co-occurred with the flexure deformation. Thus, the short-beam sensor exhibited a small voltage output owing to the large offset cancellation. In contrast, the long-beam sensor underwent a small offset, which resulted in a large voltage. Nevertheless, a sensor device with a larger deformation requires a larger chamber, which may lead to packaging difficulties and a high cost. Most devices suffer from packaging difficulties and low reliability because of the proof mass. In summary, the short- and long-beam sensors can be used to exploit particular advantages in different regions, specifically, easy packaging and a high voltage input for relatively high and low resonance frequencies, respectively.

3.3 Durability experiment

The developed vibration sensors are likely to be employed in harsh working environments, especially those involving sudden temperature changes, such as in certain vehicles and infrastructures. Thus, a durability experiment on the fabricated sensor was conducted under such conditions. A constant-climate cabinet (LHL-114, Espec Corp.) was employed to provide a suitable test environment. The durability cycle test was performed in the temperature range of 25–80 °C. One test cycle corresponded to 60 min, including the stabilization time and testing period. Three typical sensors with proof-mass diameters of 5, 4.5, and 4 mm were tested in the experiment, and the sensor outputs were recorded by the testing equipment after 180, 240, 300, 360, 420, and 480 cycles. The results demonstrated that the fabricated sensors exhibited a stable acceleration responsivity under the vibration amplitude and satisfactory performance even after severe durability testing.

4. Preliminary Application

To examine the preliminary application of the vibration sensors, an air compressor was employed as a suitable experimental platform. A commercial 3035B accelerometer sensor and one of the fabricated vibration sensors were set on the measured compressor as close as possible to avoid any influence of the sensor location (see inset of Fig. 8). Figure 8 shows the vibration response of the commercial 3035B sensor in comparison with that of the fabricated vibration sensor when subjected to the startup vibration of the compressor. When using the fabricated vibration sensor, peak random vibration signals could be effectively measured up to 15 *g*. Nevertheless, the proposed sensor exhibited a slightly asymmetric output compared with that of the commercial sensor. To overcome this problem, a specialized circuit can be employed to adjust the output baseline of the fabricated sensor.

5. Conclusions

A MEMS piezoelectric vibration sensor with a high resonance frequency and high output voltage was developed. The developed vibration sensor contained a disk proof mass attached to eight AlN C-shaped spring flexures to generate high voltage output in the high-frequency

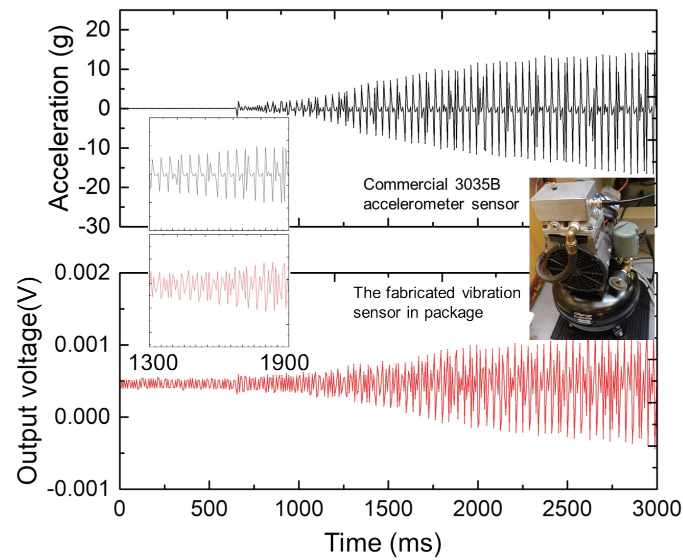

Fig. 8. (Color online) Single-sweep output for signal response to the vibrations at the top of a compressor. The outputs of a common commercial sensor (top) were compared with those of the proposed vibration sensor (bottom). Insets are the magnified signal waveform views in the range of 1300 to 1900 ms.

vibration domain. The mechanical properties and electrical performance of fabricated vibration sensors were comprehensively evaluated. The results demonstrated that the sensors exhibited an extremely high center resonance frequency of up to 6.7 kHz. An output voltage of up to 167.8 mV was achieved at an acceleration of 1 *g*.

The proposed sensor is expected to be applied in advanced civil and industrial fields owing to its specific features and satisfactory performance. The sensor design and structure can be further optimized to modify the center frequency of the resonance and improve the acceleration responsivity or output voltage.

Acknowledgments

Part of this work was conducted under one of the research topics of the New Energy and Industrial Technology Development Organization (NEDO) project named Utility Core Monitoring System Development (UCoMS).

References

1 J. Brownjohn, A. De Stefano, Y. Xu, H. Wenzel, and A. E. Aktan: J. Civ. Struct. Health Monit. **1** (2011) 79.
2 C. Tsogka, E. Daskalakis, G. Comanducci, and F. Ubertini: Comput.-Aided Civ. Infrastruct. Eng. **32** (2017) 288.
3 L. Zhang, J. Lu, R. Takei, N. Makimoto, T. Itoh, and T. Kobayashi: Rev. Sci. Instrum. **87** (2016) 085005.
4 B. O'Regan and M. Grätzel: Nature **353** (1991) 737.
5 J. Wang, M. Shahidehpour, and Z. Li: IEEE Trans. Power Syst. **23** (2008) 1319.
6 R. Takei, H. Okada, N. Makimoto, T. Itoh, and T. Kobayashi: Jpn. J. Appl. Phys. **55** (2016) 10TA06.
7 R. Takei, H. Okada, N. Makimoto, T. Itoh, and T. Kobayashi: Jpn. J. Appl. Phys. **56** (2017) 04CC03.

8 K. Kecik, A. Mitura, S. Lenci, and J. Warminski: Int. J. Non Linear Mech. **94** (2017) 200.
9 Y. Lu, E. O'Riordan, F. Cottone, S. Boisseau, D. Galayko, E. Blokhina, F. Marty, and P. Basset: J. Micromech. Microeng. **26** (2016) 124004.
10 S. Tadigadapa and K. Mateti: Meas. Sci. Technol. **20** (2009) 1.
11 B. Lee, S. Lin, W. Wu, X. Wang, P. Chang, and C. Lee: J. Micromech. Microeng. **19** (2009) 065014.
12 A. Manbachi and R. Cobbold: IEEE Sens. J. **19** (2011) 187.
13 P. Moubarak, P. Ben-Tzvi, and M. Zaghloul: IEEE Sens. J. **12** (2011) 1033.
14 H. Yu, J. Zhou, L. Deng, and Z. Wen: Sensors **14** (2014) 3323.
15 R. Elfrink, T. Kamel, M. Goedbloed, S. Matova, D. Hohlfeld, Y. Van Andel, and R. Van Schaijk: J. Micromech. Microeng. **19** (2009) 094005.
16 P. Muralt, M. Marzencki, B. Belgacem, F. Calame, and S. Basrour: Procedia Chem. **1** (2009) 1191.
17 S. Kulkarni, E. Koukharenko, R. Torah, J. Tudor, S. Beeby, T. O'Donnell, and S. Roy: Sens. Actuators, A **145** (2008) 336.
18 B. Yaghootkar, S. Azimi, and B. Bahreyni: IEEE Sens. J. 17 (2017) 4005.